The tensile properties of NiCrMo1 steel under conditions of hydrogen charging studied using the linearly increasing stress test

Qian Liu[1], **Bartolomeus Irwanto**[2], **Andrej Atrens**[1*]

[1] The University of Queensland, Materials Engineering, St Lucia, Qld 4072, Australia
[2] Alstom (Switzerland) Ltd, CH-5242 Birr, Switzerland
* Corresponding author: Andrejs.Atrens@uq.edu.au

Abstract The tensile properties of NiCrMo1 steel were investigated using the linearly increasing stress test (LIST) in air and with hydrogen charging. Hydrogen charging was carried out by applying an increasingly negative applied potential to -1550 $mV_{Ag/AgCl}$ in acidified 0.1 M Na_2SO_4, pH 2 solution. The LIST results showed that the yield stress of the steel was similar in air or with hydrogen charging. SEM examination showed that the specimens tested in air had no surface cracks, and the fracture surfaces comprised dimples. The failure in air was due to ductile overload. The specimens tested with hydrogen charging had obvious surface cracks in the necked region, and their length increased to about 550 μm with a more negative potential. However, the fracture surfaces were nevertheless dominated by ductile feature. These results imply that the influence of hydrogen was only associated with the final ductile fracture after the onset of necking.

Keywords: Steel 1, LIST 2, hydrogen embrittlement 3, SEM 4.

1. Introduction

Operation of metallic components is required in hydrogen (H) in the H economy being developed in response for the need for clean energy. The H economy requires pressure vessels resistant to hydrogen embrittlement (HE) for the production, distribution, storage and use of gaseous H_2. Though laboratory scale vessels can be made from expensive exotic materials, there are significant cost imperatives to use less expensive materials like steels in a commercial H economy. Some steels are susceptible to hydrogen, particularly high strength steels [1-11]. Some medium strength steels are resistant to hydrogen even under severe hydrogen charging conditions [12-15]. Using the linearly increasing stress test (LIST) [16], our previous investigation of 3.5NiCrMoV steel [15] showed that there was negligible influence of hydrogen on the yield stress and fracture stress, though the ductility was decreased for some tests. Detailed examination of the surface appearance and the fracture surfaces indicated that (i) there was no influence of hydrogen up to the yield stress of the steel; and (ii) hydrogen caused some small brittle fracture events in small localised areas associated with the final ductile fracture after the onset of necking. The LIST [16] is a stress-controlled version of the constant extension rate test (CERT) [17]. A LIST is identical to a CERT up to the onset of yielding, or the onset on subcritical crack growth. It is expect that the same apparent threshold stress would be measured using CERT as measured using LIST, an apparent threshold that related to the onset of plastic deformation.

The aim of this research was to evaluate using LIST the behavior of medium strength NiCrMo1 steel under hydrogen conditions. The results could be considered as a reference to the suitability of this steel for the H economy.

2. Experimental procedure

The material was the nickel chromium molybdenum steel, NiCrMo1. It is a quenched and tempered martensitic steel; the microstructure is tempered martensite as shown in Fig. 1. Table 1 presents the chemical composition. The steel was machined into specimens with 10 mm gauge length, 3 mm diameter and an overall length of 110 mm. The specimen was evaluated by LIST. The threshold stresses were measured with the potential drop (PD) measurement. LISTs were carried out in air, and in solution, (i) at the free corrosion potential (E_{corr}) and (ii) under hydrogen charging conditions.

The solution was acidified 0.1 M Na_2SO_4 pH 2 solution. Details about hydrogen charging, LIST and SEM sample preparation are as in [15]. After each LIST, the fracture surface was examined by SEM.

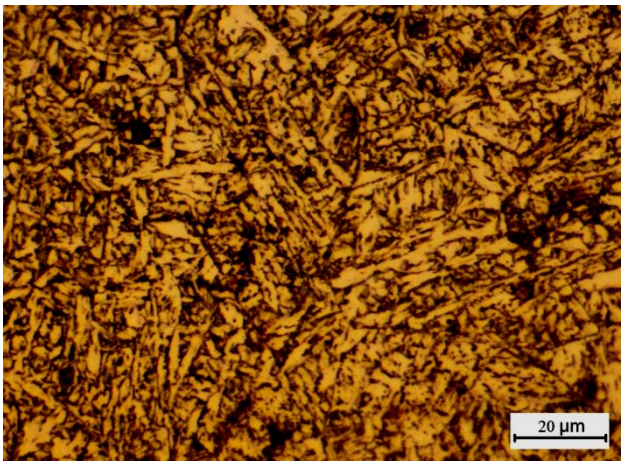

Figure 1. The microstructure of the NiCrMo1 steel.

Table 1. Chemical composition of NiCrMo1 (wt%) as determines by two independent measurements.

Steel	Composition, wt%									
	C	Ni	Cr	Mo	V	Mn	Si	S	P	Cu
NiCrMo1	0.09	1.04	0.52	0.60	0.01	0.88	0.31	0.01	0.01	0.06
	0.08	0.98	0.48	0.60	0.01	0.91	0.31	0.01	0.01	0.06

The stress rate was mostly the moderate stress rate: 0.02 MPa s^{-1}. The yield stress in air, σ_y, or the threshold stress, σ_{th}, was determined by the PD measurement. The precision for σ_y or σ_{th} was ± 5 MPa. The precision of the fracture stress was ± 2 MPa. The reduction of area, R_A, of each specimen was evaluated from the original specimen gauge diameter and the measured minimum diameter after each test. For the evaluation of σ_{th} or σ_f, in most cases the area used was the original specimen cross-section area. For tests in solution at E_{corr}, corrosion reduced the cross section area of the specimen during the LIST. In those cases, the area used was the cross section area that had undergone uniform plastic deformation.

The specimen designation can be explained by the following example: S1200.02a, where the letter ‘‘S’’ identified a specimen tested in solution (alternatively ‘‘A’’ identified a specimen tested in air), ‘‘1200’’ identified the applied potential (alternatively “ocp” identified a specimen tested in solution at the free corrosion potential), ‘‘.02’’ identified the applied stress rate, and the subsequent letter identified specimens tested under the same conditions.

3. Experimental procedure

3.1. Tensile properties

Fig. 2 shows a typical PD record for NiCrMo1 tested at 0.02 MPa s^{-1} in acidified 0.1 M Na_2SO_4 pH 2 solution at three negative potentials. Similar plots were obtained from the other experiments. Table 2 presents the measured data for σ_y, σ_{th} at which subcritical cracking appeared to initiate in solution, σ_f and R_A. The E_{corr} was about -500 $mV_{Ag/AgCl}$.

The σ_y or σ_{th} in air or at negative applied potentials were in the range of 600 to 660 MPa, while the σ_f was varied from 690 to 760 MPa. The values of R_A were about 70 ~76 %.

LIST for specimens in solution at E_{corr} produced values of the σ_{th} varying from 625 to 690 MPa, values of the σ_f varying from 710 to 800 MPa, and values of the R_A varying from 69% to 79%.

These values were comparable, or somewhat higher than, the values in air.

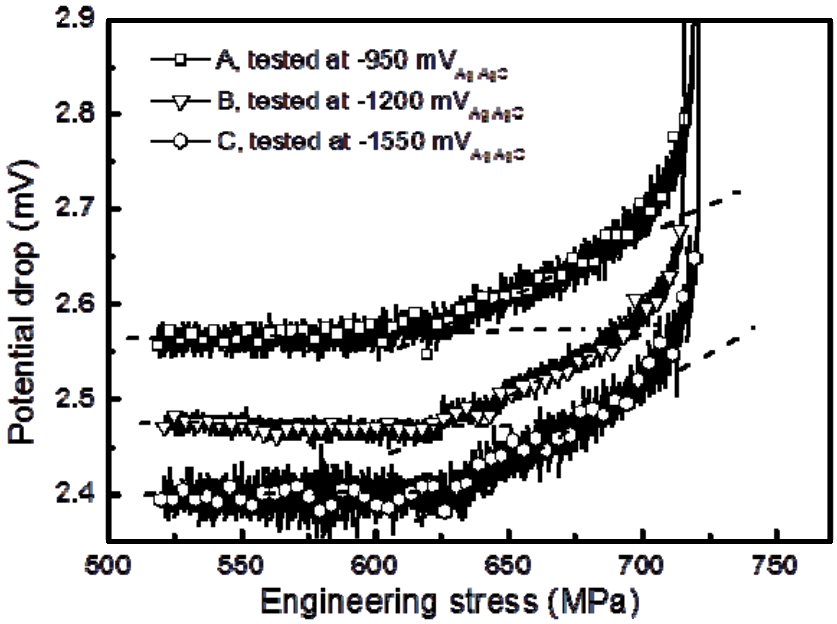

Figure 2. A typical plot of potential drop (mV) vs. engineering stress (MPa) for NiCrMo1 tested at 0.02 MPa s^{-1} in acidified 0.1 M Na_2SO_4, pH 2 solution at three potentials.

Table 2 Yield stress in air (as an engineering stress), σ_y, the apparent threshold stress at which subcritical cracking appeared to initiate in solution (as an engineering stress), σ_{th}, the fracture stress (as an engineering stress), σ_f, the reduction of area, R_A. Solution: ①0.1 M Na_2SO_4, pH=2.

Applied stress rate (MPa/s)	Sample	Solution	Applied potential ($mV_{Ag/AgCl}$)	σ_{th}±5	σ_f±2	R_A
0.02	A.02a	air	0	664	763	74%
0.02	A.02b	air	0	603	693	76%
0.02	A.02c	air	0	631	726	75%
0.02	A.02d	air	0	620	717	72%
0.002	A.002	air	0	646	740	75%
0.02	Socp.02a	①	E_{corr}	683	798	77%
0.02	Socp.02b	①	E_{corr}	625	714	79%
0.02	Socp.02c	①	E_{corr}	693	796	69%
0.02	S950.02	①	-950	619	719	73%
0.02	S1200.02	①	-1200	624	715	73%
0.02	S1400.02	①	-1400	664	759	73%
0.02	S1550.02	①	-1550	633	720	70%

3.2. Surface appearance in the necked region

Visual examination of the surface appearance of each specimen showed that there was obvious necking for all the specimens. Black corrosion products, which were easily removed by EDTA, were produced on the specimens during tests at E_{corr}. For specimens tested at negative potentials, there were cracks on the specimen surface concentrated at the fracture site.

For specimens tested in air at a rate of 0.02 MPa s^{-1}, SEM observation showed necking and shallow cracks at about 45 ° to the stress direction, and linear features parallel to the stress direction in the necked region. Specimens tested at E_{corr} showed similar surface appearance except that the surface was more rough due to corrosion.

Fig. 3 presents the surface appearances of specimens tested under hydrogen charging at 0.02 MPa

s^{-1}. Specimens tested at negative potentials showed necking, and surface cracks perpendicular to the stress direction, and cracks oriented at 45 ° to the stress direction (Fig. 3(c)). The surface cracks were concentrated at the fracture site, and the number density of cracks decreased as a function of distance from the fracture surface. The surfaces of specimens tested at negative potentials were essentially similar. Fig. 3 shows that the surface cracks increased in size with increasingly negative potential.

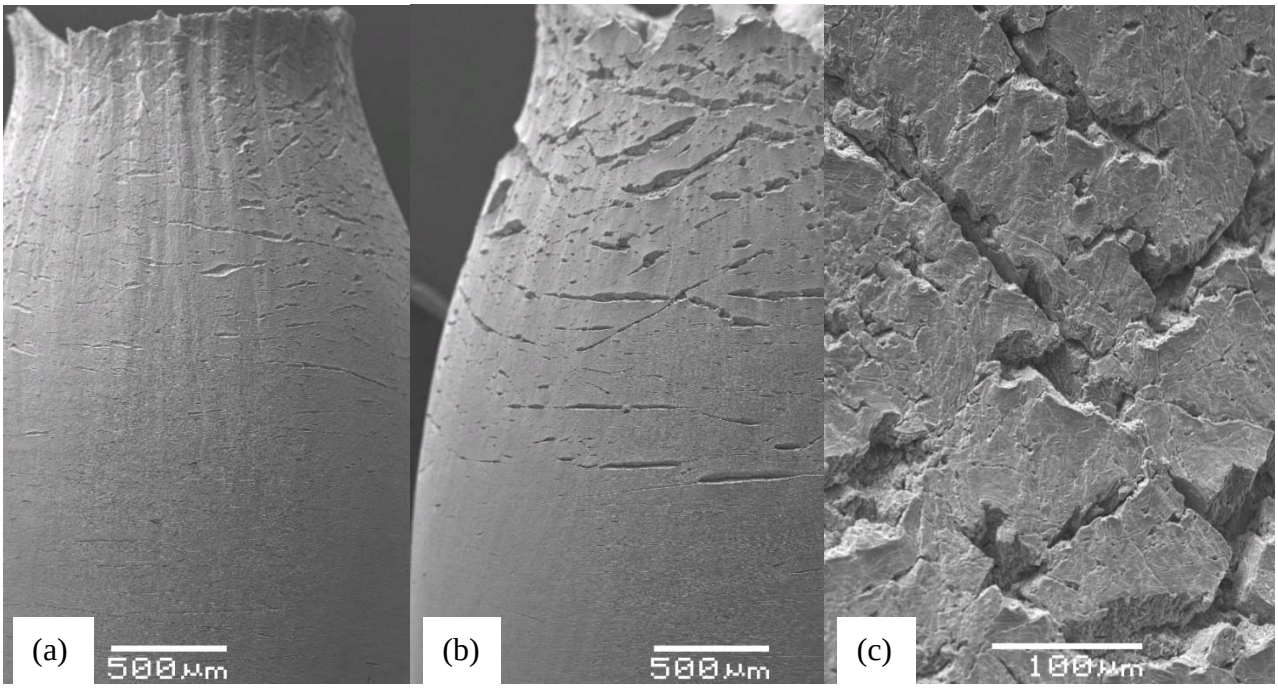

Figure 3. The surface appearances of specimens tested at negative potentials at 0.02 MPa s^{-1}. (a) -950 $mV_{Ag/AgCl}$; (b) -1550 $mV_{Ag/AgCl}$; (c) magnified view of (b) in the necked region. Tensile direction is vertical

3.3. Cross sections through fracture surface (specimen S1550.02)

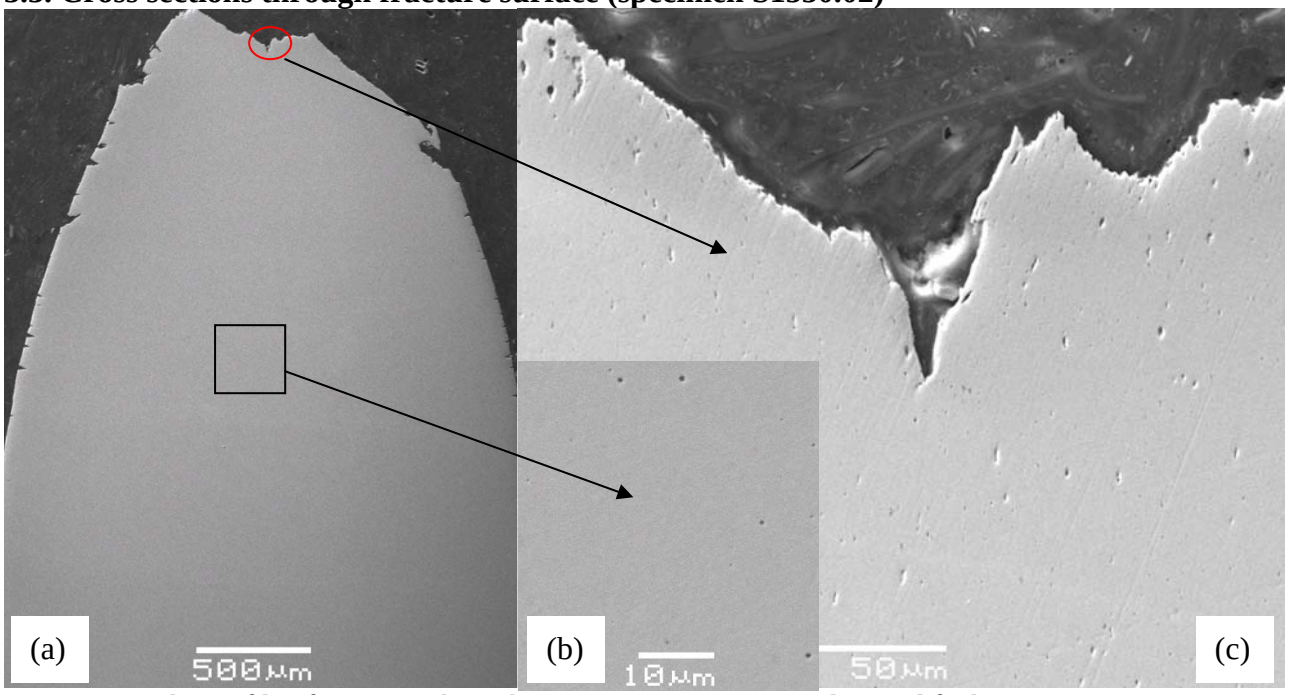

Figure 4. The profile of a section through specimen S1550.02 tested in acidified 0.1 M Na_2SO_4, pH 2 at -1550 $mV_{Ag/AgCl}$ at an applied stress rate of 0.02 MPa s^{-1}. (a) overview; (b) detailed view in the center; (c) detailed view near fracture surface. The tensile loading was in the vertical direction.

The longitudinal cross-section of specimen S1550.02 is shown in Fig. 4. Cracks initiated from the surface and extended into the specimen interior. The density of the surface cracks decreased as a function of distance from the fracture surface. Fig. 4(b) shows the detailed view in the interior of the specimen. There were small round voids, but no cracks. A magnified view of the region near the fracture surface (Fig. 4(c)) indicates that there were small holes near the fracture surface. As these sections were taken at random, it is concluded that there were no cracks in the interior of the specimens, apart from the small round voids.

3.4. SEM fractography

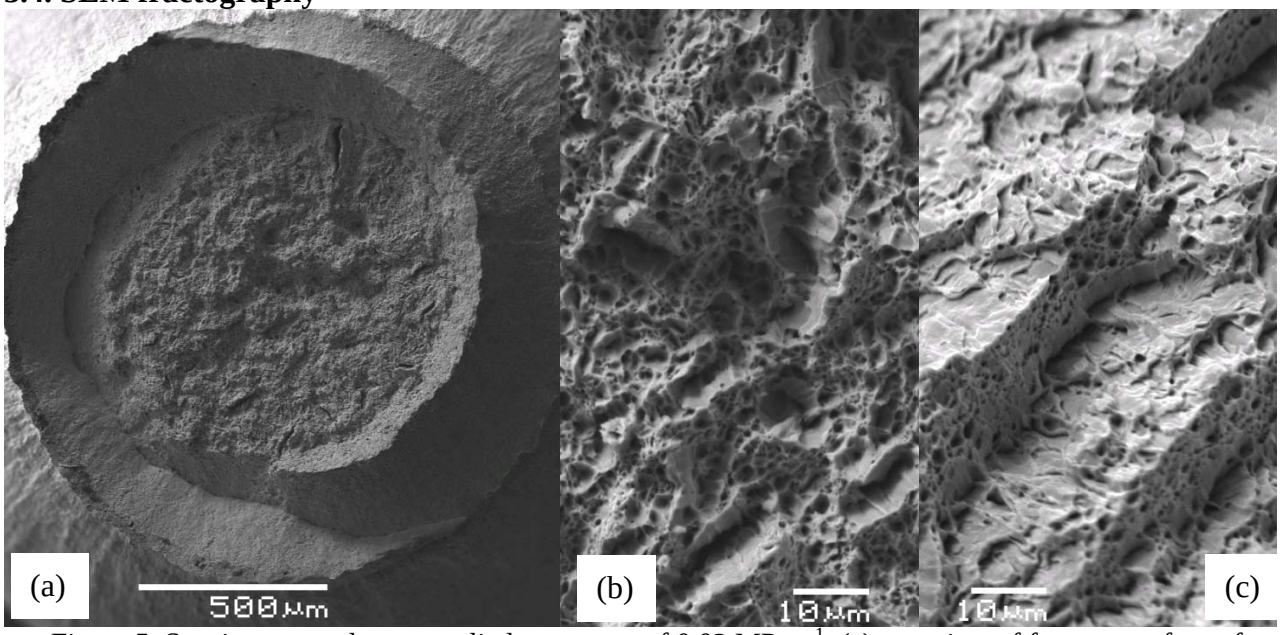

Figure 5. Specimen tested at an applied stress rate of 0.02 MPa s^{-1}: (a) overview of fracture surface of specimen A.02c, (b) a magnified view of cone part of specimen A.02c; and (c) brittle facets steps on the fracture surface of Socp.02c.

The fracture surface of specimen A.02c tested in air (Fig. 5) presented a cup and cone fracture with secondary cracks up to 140 μm in size, and showed significant ductility. These secondary cracks were surrounded by dimples, and had a small number of orientations. A magnified view of the fracture surface shown in Fig. 5 (b) indicates that the fracture surface comprised dimples, due to ductile microvoid coalescence (MVC) and secondary ductile cracks. All the secondary cracks were ductile and were surrounded by dimples. The fracture surfaces of other specimens tested in air were similar to specimen A.02c.

Similar to that obtained in air, the fracture surface of specimens Socp.02a and Socp.02b tested at E_{corr} showed a cup and cone fracture with a big secondary crack about 270 μm in size, and small secondary cracks less than 100 μm in size. However, one specimen Socp.02c tested at E_{corr} showed dimples and secondary cracks as well as some brittle facets, as shown in Fig. 5(c). Those brittle facets built up horizontal steps; dimples were like a linker between those steps. These brittle facets covered a substantial area in the middle of the fracture surface. Nevertheless, they were entirely surrounded by microvoid coalescence.

The fracture surface of specimen S950.02 tested at -950 $mV_{Ag/AgCl}$ at a rate of 0.02 MPa s^{-1} showed a cup and cone fracture as illustrated in Fig. 6. Fig. 6(b) presents a magnified view of region A, which comprised dimples and some secondary cracks. Region B at the edge, shown in Fig. 6(c), comprised brittle facets at the edge and shear dimples, i.e. dimples which had formed in the shear lips of the

cup and cone fracture at ~45° to the tensile axis, and were heavily sheared.

The fracture surfaces of specimens tested at -1200 $mV_{Ag/AgCl}$ and -1400 $mV_{Ag/AgCl}$ also showed obvious ductility, presenting a cup and cone fracture with a large secondary crack about 170 μm in size and small secondary cracks less than 150 μm in size completely surrounded by dimples.

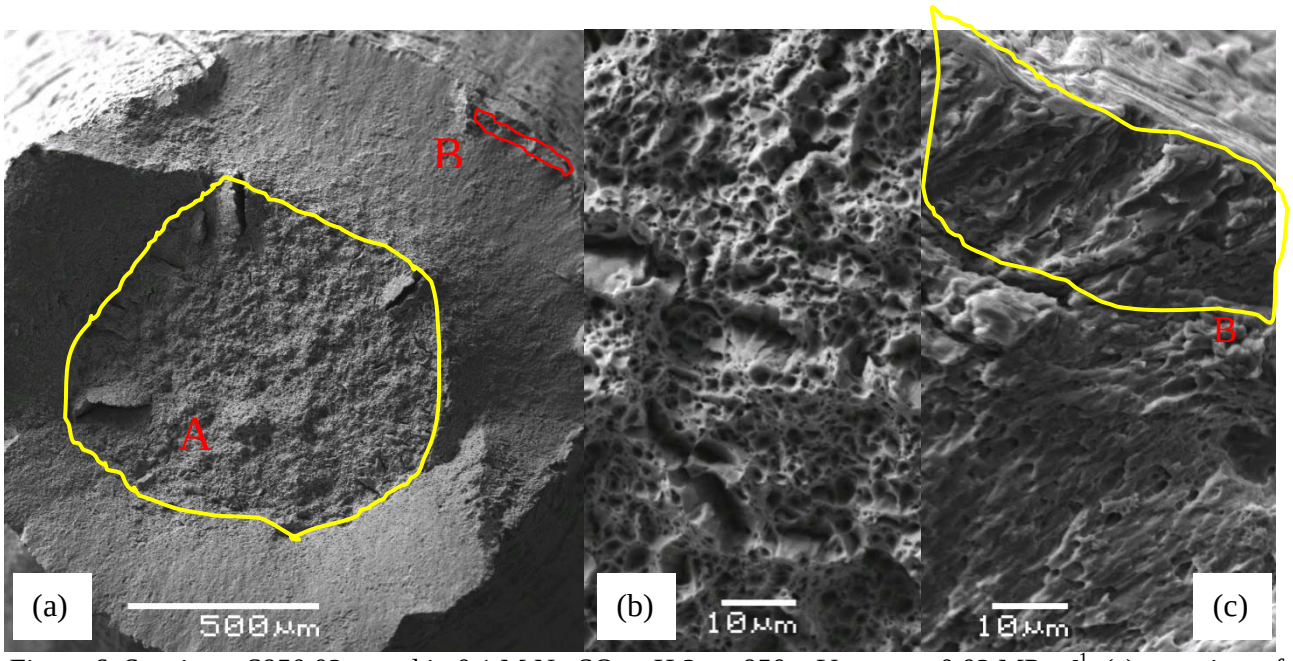

Figure 6. Specimen S950.02 tested in 0.1 M Na_2SO_4, pH 2 at -950 $mV_{Ag/AgCl}$ at 0.02 MPa s^{-1}: (a) overview of the fracture surface, (b) a magnified view of region A, and (c) a magnification of region B.

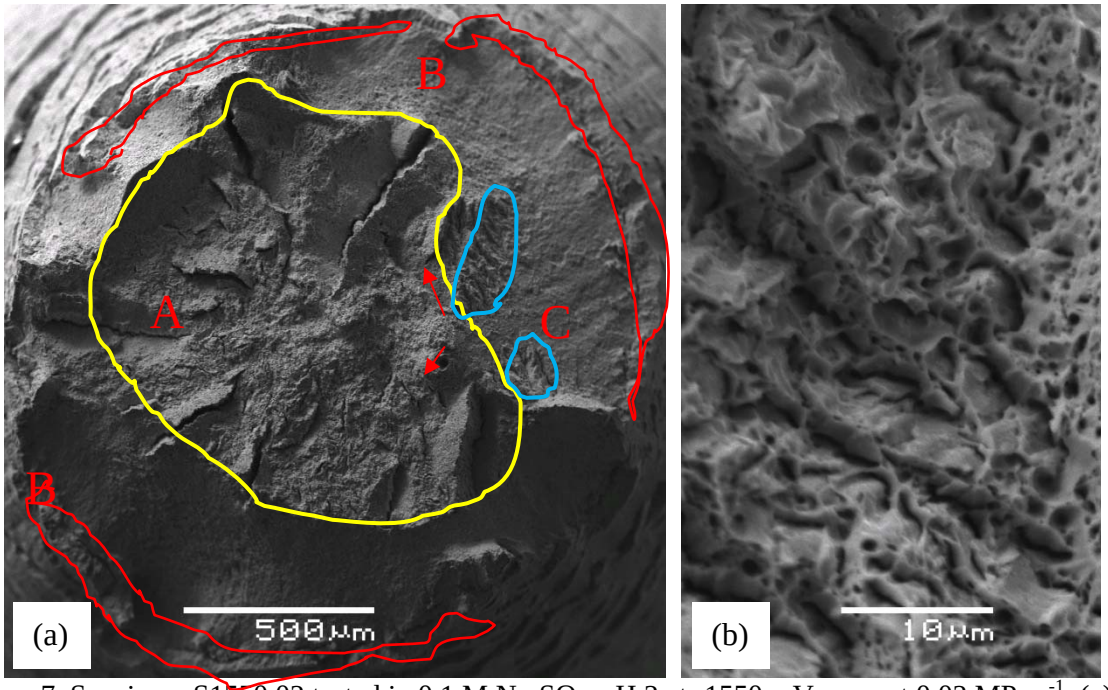

Figure 7. Specimen S1550.02 tested in 0.1 M Na_2SO_4, pH 2 at -1550 $mV_{Ag/AgCl}$ at 0.02 MPa s^{-1}: (a) an overview of the fracture surface, and (b) a detailed view in region C.

Fig. 7(a) presents the fracture surface of specimen S1550.02 tested at -1550 $mV_{Ag/AgCl}$ at a rate of 0.02 MPa s^{-1}. Region A of the fracture surface, similar to that shown in Fig. 6(b), was mainly MVC with some secondary cracks up to 550 μm. These secondary cracks surrounded by dimples were

oriented radially to the centre of the specimen. Region B was similar to that shown in Fig. 6(c). Fig. 7(b) presents a detailed view in regions C, showing small brittle facets.

4. Discussion

4.1. Tensile properties

All the specimens showed significant ductility, as demonstrated by obvious necking and high values of R_A. At the applied potentials, hydrogen was produced during each experiment at the specimen surface. The increasingly negative potentials increased the amount of H (and the H fugacity) at the specimen surface [18], and concomitantly the hydrogen concentration in the specimen. However, Table 2 indicates that decreasing applied potential did not cause any significant changes in the values of σ_{th}, σ_f and R_A. The influence of hydrogen on the tensile parameters of the NiCrMo1 steel was negligible.

4.2. Surface appearance

There were cracks at about 45° to the tensile direction on the necked surface of specimens tested in air and in solution at E_{corr}. These shallow surface cracks are attributed to the surface intersection of localised bands and stress, as the shear stress is maximum at 45 ° to the tensile direction.

For each of the specimens tested at negative potentials from -950 $mV_{Ag/AgCl}$ to -1550 $mV_{Ag/AgCl}$, there were no cracks on the surface that had undergone uniform plastic deformation, while the surface of the necked region contained cracks perpendicular to the tensile direction, and cracks about 45° to the tensile direction. The number of these cracks decreased as a function of the distance from the fracture surface. These cracks became longer with increasingly negative potential, which was attributed to high H fugacity at the specimen surface [18]. These cracks were due to the influence of hydrogen on the localized plastic deformation at the surface in the necked region of the specimen.

It can be concluded that (i) there was no hydrogen influence for stresses up to the yield stress of the material; and (ii) the influence of hydrogen was associated with localised plastic deformation and fracture. These conclusions were similar to those for the 3.5NiCrMoV steel in our previous research [15].

4.3. Cross Section

The examination of cross section of specimen S1550.02 indicated that hydrogen only had an effect (i) on the edge and places near the edge of the necked region and (ii) locations close to the fracture surface in the heavily deformed region. These facts indicate the occurrence of cracks was associated with high levels of localised plastic deformation during the process of necking during final ductile fracture. This is consistent with the results obtained from the surface appearance.

However, it is possible that the duration was not long enough for hydrogen to reach a stable concentration though the specimen, therefore, the influence of hydrogen in the centre of specimen was weaker than that of on the surface. This might provide an alternative explanation for hydrogen influence only obvious on the surface of the necked region. Nevertheless, the fact that the secondary cracks extended to the centre of the specimen tested at -1550 $mV_{Ag/AgCl}$ in Fig. 7 implies that there was sufficient hydrogen throughout the specimen under this test condition to cause hydrogen related fracture events throughout the cross section. The absence of hydrogen damage inside the specimen was not due to insufficient hydrogen inside the specimen.

4.4 Fracture surfaces

The fracture surfaces obtained in air and at E_{corr} were dominated by dimples, due to ductile

microvoid coalescence, interspersed with some secondary cracks. The difference between various specimens seems to be a slightly different amount and size of secondary cracks. These results indicated that the specimen tested in air and at E_{corr} failed due to ductile overload.

The specimens tested under negative potentials showed a significant amount of ductile features on the fracture surface, similar to those in air. Most of the substantial cracks on the fracture surfaces were oriented radially. With increasingly applied negative potential, cracks on the fracture surfaces grew longer, up to about 550 µm at -1550 $mV_{Ag/AgCl}$. However, it is hard to say that these cracks were due to hydrogen, since there were similar cracks on the fracture surfaces for specimens tested in air. The initiation of these cracks may be due to inclusions [19]. Yet the presence of hydrogen did accelerate the growth rate of these cracks.

Brittle features at the edge associated with surface cracks in the neck region were deeper at a more negative potential indicating that hydrogen had a greater influence.

There were brittle features in small localised areas in the presence of hydrogen, associated with final ductile fracture. However, these brittle features were all surrounded by regions of ductile fracture. Even at the most negative potential, the fracture surface was predominately ductile, indicating that the specimens tested under hydrogen charging also failed due to ductile overload. The influence of hydrogen was not significant.

4.5 Mechanistic interpretation

Due to (i) no measureable influence of hydrogen on the yield stress; (ii) no surface cracks in the uniformly deformed part of the specimen gauge section for any specimen, the PD technique measured the onset of plastic deformation rather than the onset of subcritical crack growth.

The influence of hydrogen was on the final fracture process after the onset of necking via two ways: (i) causing localized brittle fracture events, and (ii) accelerating crack growth rate on the fracture surface. The brittle hydrogen associated fracture events in the present study occurred simultaneously with a ductile fracture process throughout the necked region of a fracturing specimen. However, the hydrogen fracture mechanism was not comparable to the other ductile fracture mechanism attributable to the stress reaching the fracture stress, and to mechanically unstable of the specimen. The dominant fracture mechanism was ductile microvoid rupture.

There were secondary cracks on the fracture surfaces not only for the specimens tested in solution, but also from the specimens tested in air. This implies that even though these secondary cracks were accelerated by hydrogen, inclusions [19] instead of hydrogen might be responsible for the initiation of these cracks.

4.6 Implications for service

Considering the results discussed above, (i) the properties of the NiCrMo1 might be improved by reducing the inclusion density; and (ii) if the material will be used at a stress under the yield stress, the influence of hydrogen can be negligible, indicating that it is safe to use this material under the yield stress in an environment containing hydrogen for the H economy.

5. Conclusions

The tensile and fracture properties of NiCrMo1 steel under conditions of hydrogen charging were investigated by LIST and SEM. The results showed that:

1. The influence of hydrogen on the tensile parameters (σ_y, σ_{th} and R_A) was negligible;
2. There were no surface cracks in the region that had undergone uniform plastic deformation,

implying that there was no influence of hydrogen up to the yield stress of the steel;
3. There were surface cracks in the necked region on the specimens tested under hydrogen charging, implying that the influence of hydrogen was associated with the final ductile fracture process after the onset of necking.

Acknowledgements

This work is supported by an ARC linkage grant & Alstom (Switzerland) Ltd.

References

[1] S. Ramamurthy, W.M.L. Lau, A. Atrens, Influence of the applied stress rate on the stress corrosion cracking of 4340 and 3.5NiCrMoV steels under conditions of cathodic hydrogen charging, Corrosion Science, 53 (2011) 2419-2429.
[2] S. Ramamurthy, A. Atrens, The influence of applied stress rate on the stress corrosion cracking of 4340 and 3.5NiCrMoV steels in distilled water at 30 °C, Corrosion Science, 52 (2010) 1042-1051.
[3] E. Villalba, A. Atrens, Hydrogen embrittlement and rock bolt stress corrosion cracking, Engineering Failure Analysis, 16 (2009) 164-175.
[4] E. Gamboa, A. Atrens, Stress corrosion cracking fracture mechanisms in rock bolts, Journal of materials science, 38 (2003) 3813-3829.
[5] E. Gamboa, A. Atrens, Environmental influence on the stress corrosion cracking of rock bolts, Engineering Failure Analysis, 10 (2003) 521-558.
[6] R. Rieck, A. Atrens, I. Smith, The role of crack tip strain rate in the stress corrosion cracking of high strength steels in water, Metallurgical and Materials Transactions A, 20 (1989) 889-895.
[7] A. Oehlert, A. Atrens, Stress corrosion crack propagation in AerMet 100, Journal of materials science, 33 (1998) 775-781.
[8] A. Atrens, A. Oehlert, Linearly-increasing-stress testing of carbon steel in 4 N NaNO3 and in Bayer liquor, Journal of materials science, 33 (1998) 783-788.
[9] A. Atrens, Z. Wang, ESEM observations of SCC initiation for 4340 high strength steel in distilled water, Journal of materials science, 33 (1998) 405-415.
[10] M. Wang, E. Akiyama, K. Tsuzaki, Effect of hydrogen and stress concentration on the notch tensile strength of AISI 4135 steel, Materials Science and Engineering A, 398 (2005) 37-46.
[11] M. Wang, E. Akiyama, K. Tsuzaki, Effect of hydrogen on the fracture behavior of high strength steel during slow strain rate test, Corrosion Science, 49 (2007) 4081-4097.
[12] L. Marchetti, E. Herms, P. Laghoutaris, J. ChAne, Hydrogen embrittlement susceptibility of tempered 9%Cr-1%Mo steel, International Journal of Hydrogen Energy, 36 (2011) 15880.
[13] E. Villalba, A. Atrens, An evaluation of steels subjected to rock bolt SCC conditions, Engineering Failure Analysis, 14 (2007) 1351-1393.
[14] E. Villalba, A. Atrens, SCC of commercial steels exposed to high hydrogen fugacity, Engineering Failure Analysis, 15 (2008) 617-641.
[15] Q. Liu, B. Irwanto, A. Atrens, The influence of hydrogen on 3.5NiCrMoV steel studied using the linearly increasing stress test, Corrosion Science, (2012) DOI: 10.1016/j.corsci.2012.10.019.
[16] A. Atrens, C. Brosnan, S. Ramamurthy, A. Oehlert, I. Smith, Linearly increasing stress test (LIST) for SCC research, Measurement Science and Technology, 4 (1993) 1281.
[17] N. Winzer, A. Atrens, W. Dietzel, G. Song, K. Kainer, Comparison of the linearly increasing stress test and the constant extension rate test in the evaluation of transgranular stress corrosion

cracking of magnesium, Materials Science and Engineering: A, 472 (2008) 97-106.
[18] A. Atrens, D. Mezzanotte, N.F. Fiore, M.A. Genshaw, Electrochemical studies of hydrogen diffusion and permeability in Ni, Corrosion Science, 20 (1980) 673-684.
[19] K. Yoshino, C. McMahon, The cooperative relation between temper embrittlement and hydrogen embrittlement in a high strength steel, Metallurgical and Materials Transactions B, 5 (1974) 363-370.
[20] A.M. Brass, J. Chêne, Influence of tensile straining on the permeation of hydrogen in low alloy Cr–Mo steels, Corrosion Science, 48 (2006) 481-497.
[21] M. Hashimoto, R. Latanision, Theoretical study of hydrogen transport during plastic deformation in iron, Acta Metallurgica, 36 (1988) 1837-1854.